ADVANCED FUNCTIONAL MATERIALS
www.afm-journal.de

Tuning the Electronic Bandgap of Graphdiyne by H-Substitution to Promote Interfacial Charge Carrier Separation for Enhanced Photocatalytic Hydrogen Production

*Jian Li, Amine Slassi, Xu Han, David Cornil, Minh-Huong Ha-Thi, Thomas Pino, Damien P. Debecker, Christophe Colbeau-Justin, Jordi Arbiol, Jérôme Cornil, and Mohamed Nawfal Ghazzal**

Graphdiyne (GDY), which features a highly π-conjugated structure, direct bandgap, and high charge carrier mobility, presents the major requirements for photocatalysis. Up to now, all photocatalytic studies are performed without paying too much attention to the GDY bandgap (1.1 eV at the G_0W_0 many-body theory level). Such a narrow bandgap is not suitable for the band alignment between GDY and other semiconductors, making it difficult to achieve efficient photogenerated charge carrier separation. Herein, for the first time, it is demonstrated that tuning the electronic bandgap of GDY via H-substitution (H-GDY) promotes interfacial charge separation and improves photocatalytic H_2 evolution. The H-GDY exhibits an increased bandgap energy (≈2.5 eV) and exploitable conduction band minimum and valence band maximum edges. As a representative semiconductor, TiO_2 is hybridized with both H-GDY and GDY to fabricate a heterojunction. Compared to the GDY/TiO_2, the H-GDY/TiO_2 heterojunction leads to a remarkable enhancement of the photocatalytic H_2 generation by 1.35 times under UV–visible illumination (6200 µmol h^{-1} g^{-1}) and four times under visible light (670 µmol h^{-1} g^{-1}). Such enhancement is attributed to the suitable band alignment between H-GDY and TiO_2, which efficiently promotes the photogenerated electron and hole separation, as supported by density functional theory calculations.

1. Introduction

In a response to the urgent need for sustainable and clean energy source for the upcoming generations, photocatalytic hydrogen evolution involving light-irradiated semiconductors offers both a sustainable and relatively low-cost solution.[1–7] Along with the intensive research efforts in developing photocatalysts with high performance, low cost, and environmental friendliness, carbon-based hybrid photocatalysts represented by graphene have emerged as a new alternative class of materials.[8,9] To maximize the charge carrier transport and separation, graphene-based hybrid photocatalysts require a preliminary opening of its zero bandgap, by either chemical modification or electric field control.[10,11] Compared to graphene, graphdiyne (GDY), a rapidly developing 2D carbon material, is an even more promising candidate for catalytic energy conversion, owing to its inherent direct bandgap, high charge carrier mobility, and simple preparation methods.[12–20] Up to

Dr. J. Li, Prof. C. Colbeau-Justin, Dr. M. N. Ghazzal
Université Paris-Saclay
UMR 8000 CNRS
Institut de Chimie Physique
Orsay 91405, France
E-mail: mohamed-nawfal.ghazzal@universite-paris-saclay.fr
Dr. A. Slassi, Dr. D. Cornil, Prof. J. Cornil
Laboratory for Chemistry of Novel Materials
University of Mons
Place du Parc 20, Mons 7000, Belgium
X. Han, Prof. J. Arbiol
Catalan Institute of Nanoscience and Nanotechnology (ICN2)
CSIC and BIST
Campus UAB, Bellaterra, Barcelona, Catalonia 08193, Spain
The ORCID identification number(s) for the author(s) of this article can be found under https://doi.org/10.1002/adfm.202100994.
Dr. M.-H. Ha-Thi, Dr. T. Pino
Université Paris-Saclay
CNRS
Institut des Sciences Moléculaires d'Orsay
Orsay 91405, France
Prof. D. P. Debecker
Institute of Condensed Matter and Nanosciences (IMCN)
UCLouvain
Place L. Pasteur 1, 1348 Louvain-la-Neuve, Belgium
Prof. J. Arbiol
ICREA
Pg. Lluís Companys 23, Barcelona, Catalonia 08010, Spain

DOI: 10.1002/adfm.202100994

date, semiconductors including TiO_2, ZnO, CdS, and C_3N_4 have been successfully hybridized with GDY for enhanced photocatalytic applications.[21–26] However, all these photocatalytic systems were developed without any optimization of the GDY bandgap. The narrow bandgap (around 1.1 eV at the theoretical level) of pristine GDY neither meets the requirement to overcome the theoretical endothermic change in the process of water splitting (i.e., 1.23 eV),[27,28] nor achieve the interfacial separation of photogenerated charge carriers to the maximum extent, because of the poor mismatch between the conduction/valence band edges of GDY and the donating/accepting energy levels of the other semiconductor. Tuning the bandgap of GDY in a hybrid system would provide a photosynthetic platform to mimic the "natural photosynthesis" for efficient hydrogen evolution. Type II heterostructured photocatalysts that possess adequate band alignment between two semiconductors are demonstrated to spatially separate the photogenerated charge carriers for highly efficient water reduction and oxidation to achieve water splitting.[29,30] Thus, tuning the electronic bandgap of GDY, to fabricate such a type II heterostructure, represents a great potential for developing high-performance photocatalysts.

Chemical modification and element doping have been considered as effective approaches for adjusting the electronic band structure and related properties of carbon allotropes.[31–34] The traditional "top-down" doping method requires high temperature treatment under a specific atmosphere containing the heteroatom source, which is hard to control in terms of doping sites (at either the acetylene moieties or the benzene rings) to achieve the targeted properties. Owing to the unique solution-synthesis method of GDY,[35–40] a controllable doping/substitution method using a monomer design strategy provides an ideal bottom-up solution for adjusting the electronic bandgap of GDY. Hydrogen-substituted graphdiyne (H-GDY), prepared by the coupling reaction of 1,3,5-triethynylbenzene monomer, appears to be a good candidate. On the one hand, the introduction of hydrogen atoms on the meta-positions of benzene rings maintains the large π-conjugated structure and excellent charge carrier mobility.[41] On the other hand, the introduction of H atoms has been demonstrated to enable enlarging the bandgap of carbon-based materials,[42,43] which is beneficial to target the construction of type II heterostructured photocatalysts.

Toward this end, H-GDY was prepared through the polymerization of 1,3,5-triethynylbenzene monomer using CuCl as a catalyst. Experiments and theoretical calculations indicated that H-GDY possessed a bandgap energy of ≈2.5 eV and exploitable conduction band minimum (CBM) and valence band maximum (VBM) edges. As a proof of concept, TiO_2 was combined with H-GDY to fabricate a type II heterostructured photocatalyst. The H-GDY/TiO_2 heterojunction showed remarkable photocatalytic activity for H_2 generation, under both UV–visible and visible light excitation. Density functional theory (DFT) calculations attribute this enhancement to the suitable band alignment between H-GDY and TiO_2, which promotes the interfacial separation of the photogenerated electrons and holes and the photosensitization of TiO_2 under visible light. Time-resolved microwave conductivity (TRMC) measurements confirmed a longer charge carrier lifetime for H-GDY/TiO_2 (≈0.33 µs), compared to GDY/TiO_2 (≈0.24 µs), further evidencing an efficient interfacial charge separation between H-GDY and TiO_2. The concept of tuning the electronic bandgap of GDY to promote interfacial charge separation opens a new avenue for GDY-based photocatalysts.

2. Results and Discussion

We have first characterized the electronic structure of an isolated sheet of H-GDY versus GDY at the DFT level using periodic boundary conditions and the Perdew–Burke–Ernzerhof (PBE) functional within the generalized gradient approximation (GGA). The main goal here is to describe on a relative basis the changes in the electronic structure when going from GDY to H-GDY. **Figure 1** displays the band structure and the

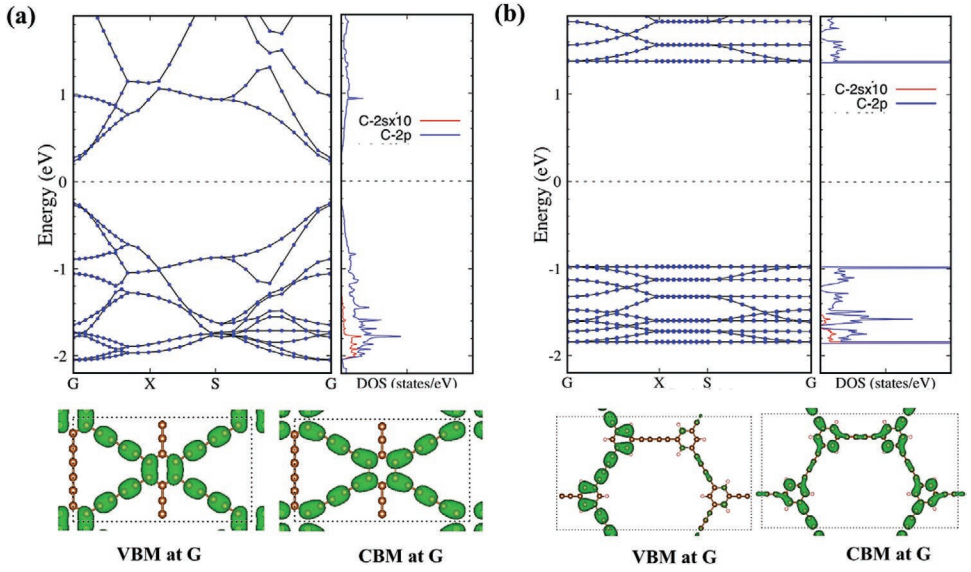

Figure 1. Band structure and projected density of states on the carbon orbitals of a) GDY and b) H-GDY calculated at the DFT level and shape of the HOMO and LUMO levels of the unit cell.

corresponding density of states (DOS) together with the shape of the highest occupied molecular orbital (HOMO) and lowest unoccupied molecular orbital (LUMO) of the unit cell. The bandgap of GDY is calculated to be 0.46 eV and the width of the valence band to be 1.81 eV, in good agreement with previous calculations.[27,28] As expected, the bandgap calculated at the PBE level is lower than the quasi-particle bandgap of 1.1 eV found at the GW many-body theory level owing to the well-established underestimation of electronic bandgaps with GGA functionals. Nevertheless, comparing at the GGA level the relative values of the bandgap of two different materials and the relative alignment of their valence or conduction band edges are meaningful, which will not thus affect the interpretation of the experimental results based on our calculations. The theoretical results reveal that the hydrogenation of graphdiyne (H-GDY) induces the opening of the bandgap up to 2.40 eV, while the width of valence band is reduced down to 0.82 eV. Those trends are rationalized by the fact that all benzene rings are connected in meta positions in H-GDY, thus limiting the degree of conjugation and hence increasing the gap. Such change is also expected to impact the electronic coupling between the unit cells and hence the mobility of the charge carriers, as evidenced by the flattening of the CB and VB edges in Figure 1b. The positions of the VB and CB edges of GDY (H-GDY) are calculated to be –4.92 and –5.37 eV (–3.50 and –5.83 eV), respectively, which translates into a downward shift by 1.42 eV of the VB edge and an upward shift by 0.46 eV of the CB edge when going from GDY to H-GDY.

H-GDY was then synthesized via the coupling reaction of 1,3,5-triethynylbenzene monomer. In brief, 1,3,5-triethynylbenzene and CuCl were firstly added in pyridine and then heated at 60 °C for 24 h (**Figure 2**a). The presence of oxygen stimulated the formation of Cu I/II species, which catalyzed the coupling reactions of the monomer to yield a yellowish powder (H-GDY). Raman spectroscopy, a useful technique for carbon materials, was used to study the bonding structure of the prepared H-GDY. Compared to the terminal C≡C stretching mode at 2123 cm^{-1} in the monomer (Figure S1, Supporting Information), the shifted peak at 2224 cm^{-1} in H-GDY confirmed the successful formation of conjugated diacetylenic linkages (Figure 2b). The peaks located at 997 and 1589 cm^{-1} are attributed to the ring breathing and ring stretching of aromatic moieties, respectively.[44] Transmission electron microscopy (TEM) displayed that the prepared H-GDY was composed of dispersed thin layers, which is beneficial to the adsorption of solvent and fast charge transfer (Figure S2, Supporting Information). X-ray photoelectron spectroscopy (XPS) revealed that the prepared H-GDY powder mainly contained elemental carbon and oxygen while no Cu species were detected, indicating that they were successfully removed

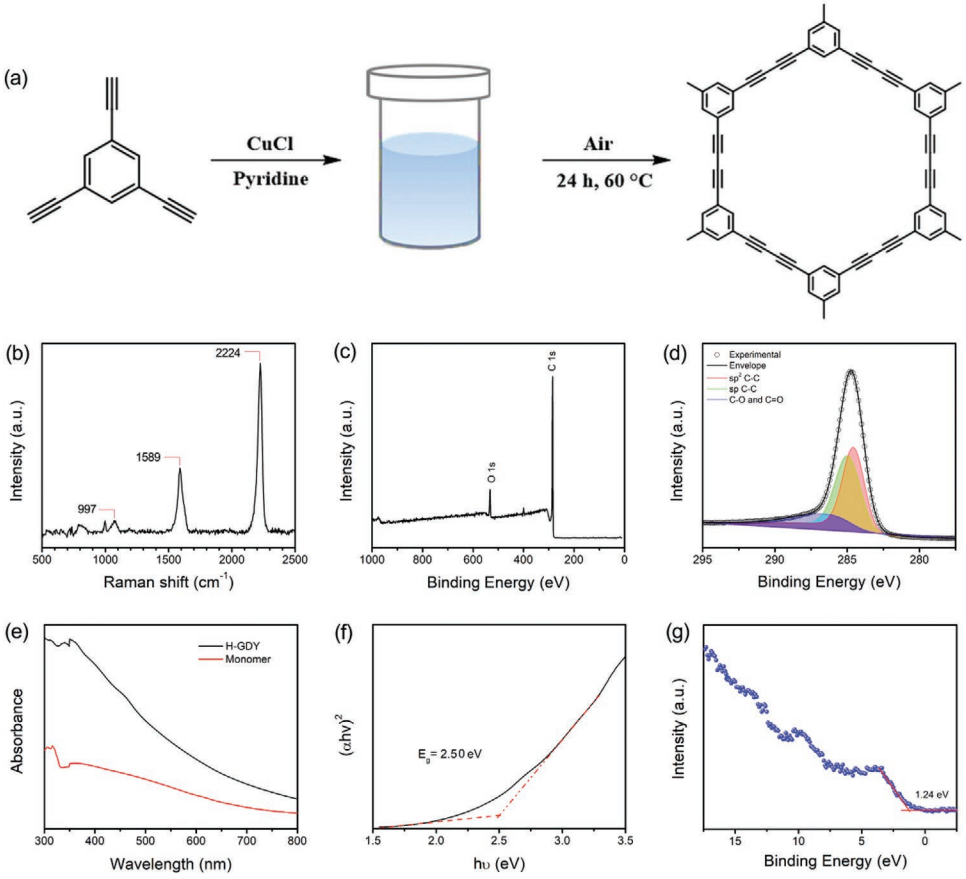

Figure 2. Synthesis and characterization of H-GDY. a) Schematic illustration of the synthesis of H-GDY powder; b) Raman spectrum of H-GDY; c) XPS survey spectrum and d) high-resolution C 1s spectrum of H-GDY; e) UV–vis absorption spectrum and f) Tauc plot of H-GDY; g) high-resolution XPS valence band spectrum of H-GDY.

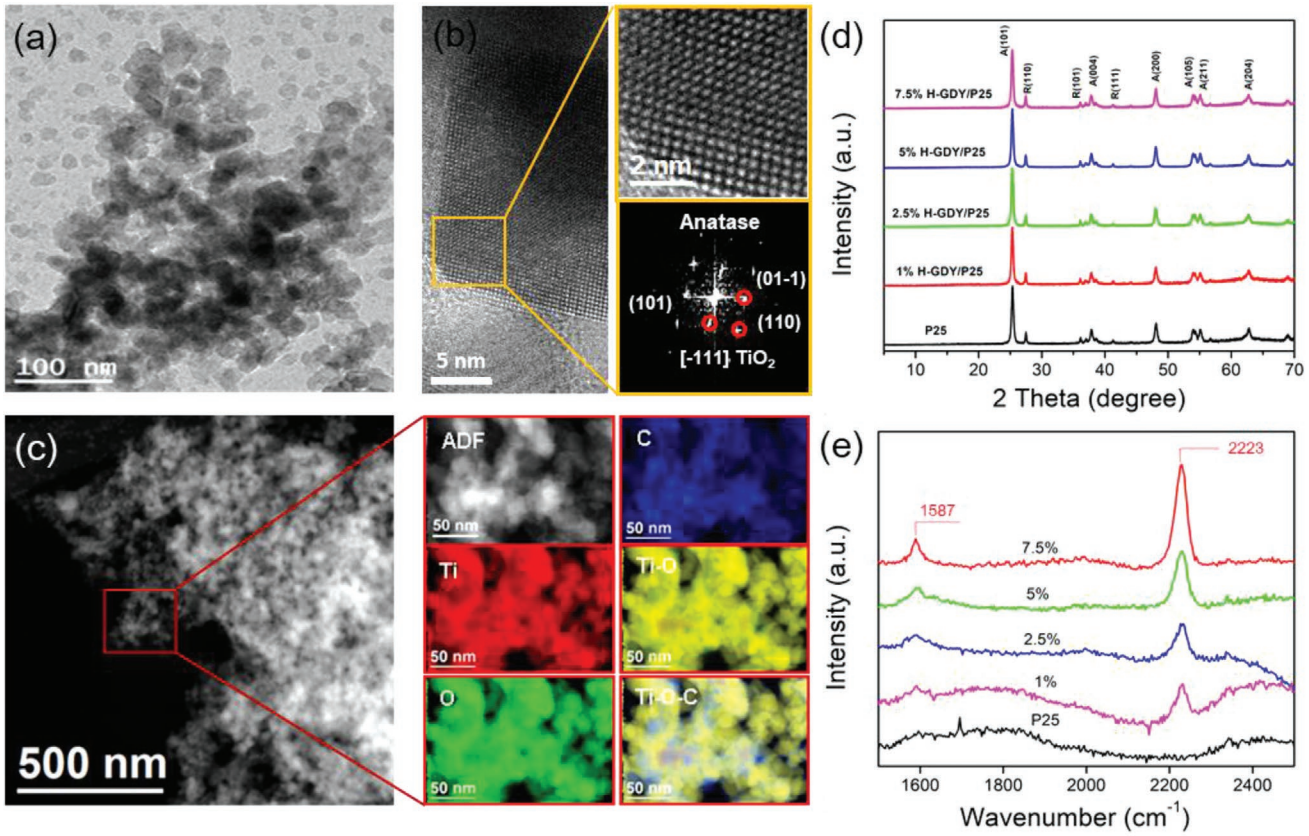

Figure 3. Characterization of H-GDY/TiO_2; a) TEM image of 5% H-GDY/TiO_2; b) HRTEM image, detail of the orange squared region and its corresponding power spectrum; c) EELS mapping of selected region in 5% H-GDY/TiO_2; d) XRD patterns and e) Raman spectra of TiO_2 and H-GDY/TiO_2 with different contents of H-GDY.

(Figure 2c). Deconvolution of the high-resolution C 1s spectra displayed the major fractions of sp and sp2 hybridized carbons with binding energies at 284.5 and 285.1 eV, respectively (Figure 2d). The additional oxygen atoms could originate from the partial oxidation of terminal alkyne units. In comparison to the monomer, an obvious bathochromic shift was observed in the UV–visible spectrum (Figure 2e), suggesting enlarged electron delocalization by the extended π-conjugated system. The optical bandgap (E_g) estimated from the Tauc plot is 2.50 eV (Figure 2f), which is in agreement with the DFT calculations. Such a bandgap is large enough to overcome the theoretical endothermic change associated to the process of water splitting (i.e., 1.23 eV). The valence band edge of H-GDY was determined by high-resolution XPS to be 1.24 V vs normal hydrogen electrode (NHE) (Figure 2g). Combined to the bandgap of 2.50 eV, the conduction band and valence band edges of H-GDY are calculated at −1.26 and 1.24 V vs NHE (−3.24 and −5.74 eV vs vacuum level), respectively. It is noted that there is a slight difference between the DFT calculations and the experimental determination of the bandgap, CB and VB energy levels, which is probably because of defects and intersheet interactions in the samples.

To demonstrate the potential of tuning the bandgap of GDY by H-substitution to fabricate type II heterojunction, TiO_2 was chosen as a model semiconductor to be interfaced with H-GDY. The microstructure of H-GDY/TiO_2 composite was firstly characterized by transmission electron microscopy (TEM). The images indicated that the TiO_2 nanoparticles were dispersed with particle size of tens of nanometers (**Figure 3**a). The high-resolution TEM (HRTEM) image revealed that TiO_2 and H-GDY were tightly connected, indicating the successful formation of the heterojunction (Figure S3, Supporting Information). TiO_2 nanoparticle has a crystal phase in agreement with TiO_2 anatase (space group = I41/AMDS) with a = 3.7850 Å, b = 3.7850 Å, and c = 9.5140 Å (Figure 3b). The electron energy loss spectroscopy (EELS) compositional mapping of the selected region displayed a homogeneous distribution of both Ti and O. The spatial distribution of C was different from that of Ti and O elements, indicating that the sample had two composite phases (Figure 3c). X-ray diffraction (XRD), Raman spectra, and XPS were performed to investigate the composition and chemical state of H-GDY/TiO_2 composite. The XRD of TiO_2 exhibited a mixture of anatase and rutile crystalline phase, typical of P25, with the anatase (101) preferential orientation. No typical diffraction patterns for H-GDY were observed, probably owing to their relatively low amount and crystallinity (Figure 3d). Compared to pristine TiO_2, the H-GDY/TiO_2 composites exhibit enhanced characteristic peaks of H-GDY at 1587 and 2223 cm^{-1} with the increase of H-GDY content, confirming the successful blending (Figure 3e). The high-resolution Ti 2p peak for H-GDY/TiO_2 was resolved at the same binding energy, indicating that the valence band states of Ti have not changed upon coupling (Figure S4, Supporting

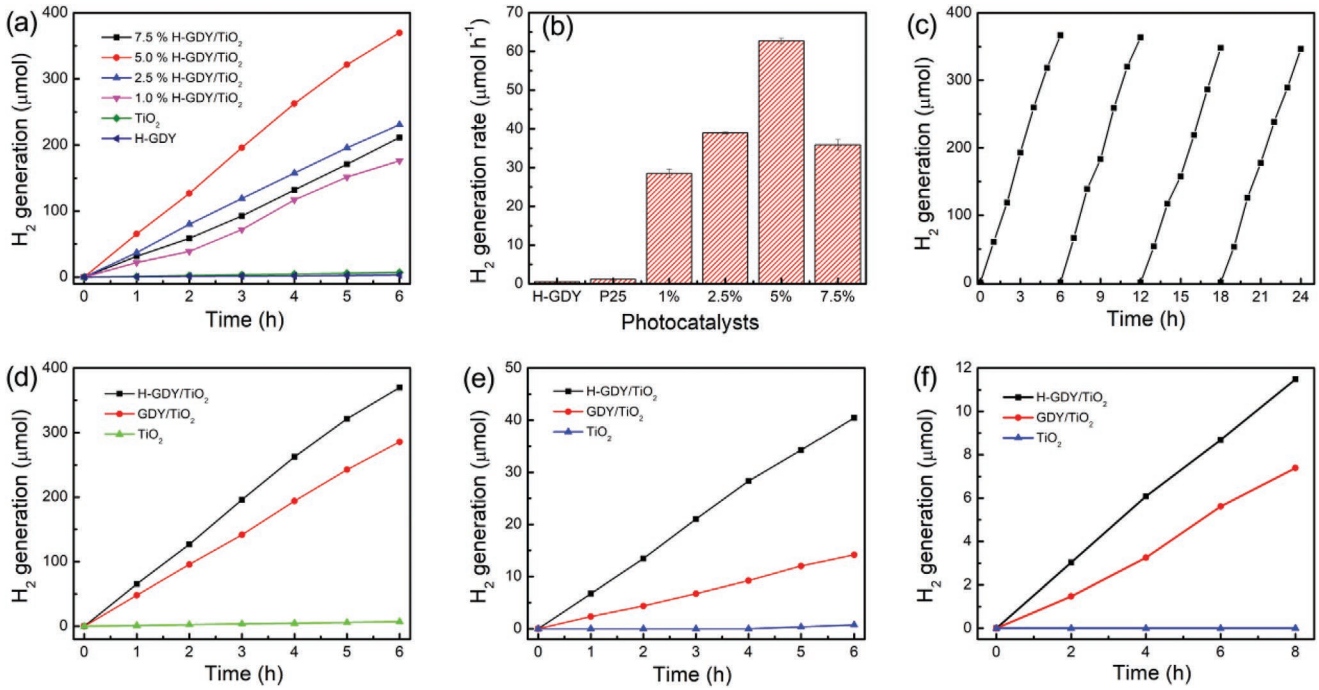

Figure 4. Photocatalytic characterization of different samples. a) Photocatalytic activity and b) H_2 generation rate for H-GDY/TiO_2 composites with different contents; c) stability test of 5% H-GDY/TiO_2 photocatalyst; d) photocatalytic activity of H-GDY/TiO_2, GDY/TiO_2, and TiO_2 composites under xenon lamp illumination; e) photocatalytic activity of H-GDY/TiO_2, GDY/TiO_2, and TiO_2 composites under visible light illumination (xenon lamp equipped with 405 filter); f) photocatalytic activity of H-GDY/TiO_2, GDY/TiO_2, and TiO_2 composites in pure water under xenon lamp illumination.

Information). UV–visible diffuse reflectance spectra demonstrated that the introduction of H-GDY redshifted the absorption of TiO_2 (Figure S5, Supporting Information).

The photocatalytic activity of the H-GDY/TiO_2 nanocomposite was evaluated toward H_2 generation in methanol/water solution (1:3 v/v) under xenon lamp illumination. The photocatalytic activity of pristine TiO_2, which showed negligible H_2 generation, was improved remarkably when mixed with H-GDY. The photocatalytic activity increased with the content of H-GDY and reached an optimal efficiency for 5% H-GDY/TiO_2 (**Figure 4**a). The total amount of H_2 generated is up to 370 μmol after 6 h, corresponding to ≈6200 μmol h^{-1} g^{-1} H_2 production rate (Figure 4b). A further increase in the H-GDY content reduces the photocatalytic performance. This result suggests that a higher coverage of the TiO_2 surface reduces the accessibility to the active sites on the TiO_2 surface. To assess the stability of the photocatalysts, the optimal 5% H-GDY/TiO_2 sample was subjected to four consecutive test cycles of hydrogen evolution (Figure 4c). The 5% H-GDY/TiO_2 sustained a stable photoactivity for hydrogen evolution after four cycles under identical experimental conditions.

For comparison, GDY was synthesized and hybridized with TiO_2 under the same conditions. The hybridization of GDY and TiO_2 was also characterized, and the Raman spectra and HRTEM images of 5% GDY/TiO_2 were presented in Figures S6 and S7 (Supporting Information). Both H-GDY/TiO_2 and GDY/TiO_2 composites displayed much higher photocatalytic activities than that of pure TiO_2 (Figure 4d,e), which is attributed to the synergetic charge transfer processes in the composites. Notably, the H_2 generated rates of the 5% H-GDY/TiO_2 were 1.35 and 4 times higher than those of the 5% GDY/TiO_2 under UV–visible and visible light, respectively. To shine light on the reason for the enhanced photoactivity, the absorption spectra of H-GDY/TiO_2 and GDY/TiO_2 were compared. The GDY/TiO_2 exhibited larger absorption in the visible range (Figure S8, Supporting Information), which indicated that the higher photoactivity of H-GDY/TiO_2 was attributed to the efficient interfacial charge separation instead of the large range of light absorbance. Excitingly, the H-GDY/TiO_2 even generate nearly 11 μmol H_2 from pure water after 8 h illumination, nearly 1.6 times that of GDY/TiO_2 (Figure 4f), further indicating the great potential of bandgap engineering of GDY for enhancing the photocatalytic efficiency.

DFT calculations were performed to shine light on the effect of H-substitution of the GDY on the properties of the hybrid systems made with TiO_2. For the sake of comparison with our experimental observations, we considered electron transfer processes only over the main exposed surface (101) of TiO_2, which is nonpolar and exhibits superior activity for photoreduction reactions.[45,46] The optimized structures of the built TiO_2/GDY (H-GDY) interfaces are given in Figure S9 (Supporting Information) and the projected band structure of the hybrid system in Figure S10 (Supporting Information). We have calculated at DFT/PBE level with van der Waals corrections the interaction energy between the two components by the following equation

$$E_{\text{int}} = (E_{\text{tot}} - E_{\text{TiO}_2} - E_{\left(\frac{\text{GDY}}{\text{H}} - \text{GDY}\right)})/A \quad (1)$$

where E_{tot}, E_{TiO_2}, and $E_{\left(\frac{\text{GDY}}{\text{H}} - \text{GDY}\right)}$ are the total energies of the heterostructure, individual TiO_2, and individual GDY (H-GDY) layers, respectively, in the geometry of the fully relaxed heterostructure, and A is the area of the interface.

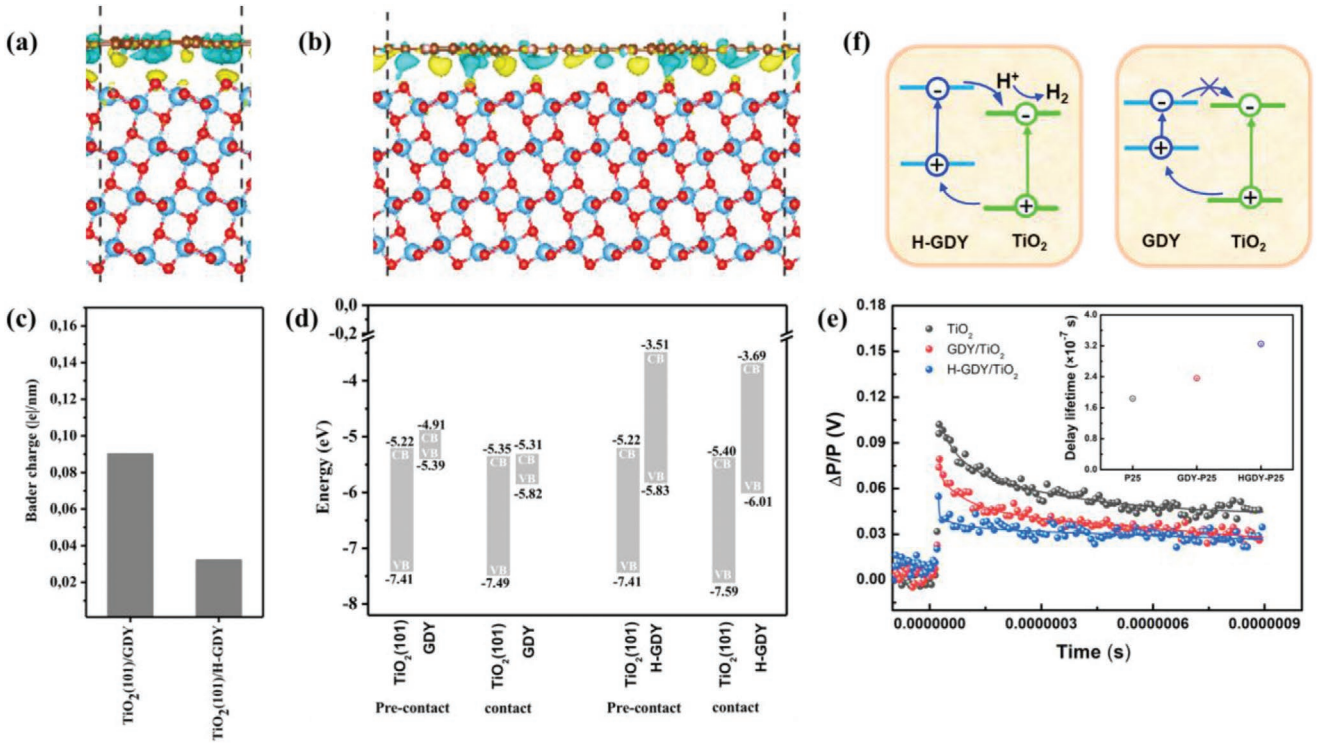

Figure 5. Side views of the 3D charge density difference in the a) TiO_2(101)/GDY and b) TiO_2(101)/H-GDY heterostructures; isosurface values for 3D charge density difference plots are 0.09 e $Å^{-3}$; the accumulation and depletion of electrons are represented in cyan and yellow, respectively; c) calculated Bader charge accumulated on the GDY (H-GDY) monolayer in the heterostructure; d) relative band alignment of VB and CB band edges before and after the formation of the heterostructure. e) TRMC measurements of TiO_2, GDY/TiO_2, and H-GDY/TiO_2 at 360 nm excitation wavelength; inset: the fitting of the decay lifetime of the three samples; f) schematic illustration of the interfacial charge transfer between TiO_2 and H-GDY/GDY.

The GDY (H-GDY) monolayer and the top layer of the TiO_2 surface undergo only a negligible buckling at the interfaces. The distance between H-GDY and TiO_2 (2.57 Å) is smaller than that computed between GDY and TiO_2 (2.75 Å). The calculated binding energies are found to be relatively comparable in TiO_2/GDY and TiO_2/H-GDY heterostructures (–7.32 meV $Å^{-2}$ vs –4.20 meV $Å^{-2}$ per unit cell, respectively). This points that the H-substituted GDY does not perturb thermodynamically the interaction with TiO_2.

The amount of interfacial charge transfer in the ground state in the two different systems has been quantified by using a Bader charge analysis (**Figure 5**c). In both cases, there is a charge transfer in the ground state between the two components, with the positive charge systematically localized in the H-GDY or GDY monolayer while the negative charge is localized in the TiO_2 slab, acting thus as the acceptor layer. This trend is rationalized by the small energy difference between the VB edge of GDY/H-GDY with respect to the CB edge of TiO_2. Interestingly, although the size of unit cell is smaller when considering GDY, the hole accumulation in GDY in the ground state is larger than that in H-GDY, most probably owing to the larger carbon areal density in GDY; this is in full consistency with the larger binding energy computed for the GDY/TiO_2 hybrid system. The pronounced hole accumulation in GDY also explains the large downward shifts of the VB and CB edges when going from the individual components to the blend (Figure 5d). It is also of prime interest to analyze the alignment of the band edges, which are key parameters that govern the charge transfer processes at the interfaces. As shown in Figure 5d, there is a large valence band offset ΔE_{VB} in the GDY/TiO_2 heterostructure while the CBM of GDY is lying very close to that of TiO_2. Under UV–visible light excitation of TiO_2, charges can be generated following an efficient photoinduced hole transfer between the valence bands of the two components whereas electron transfer processes between the conduction bands are expected to be much less efficient owing to the absence of a significant driving force. For H-GDY/TiO_2 interfaces, there is a large offset between both the CBM and VBM of the two layers, leading to a type II band alignment; photogenerated charge carriers are thus expected to be observed, originating from both efficient photoinduced hole transfer processes between the valence bands (from TiO_2 to H-GDY) upon photoexcitation of TiO_2 and efficient photoinduced electron transfer processes between the conduction bands (from H-GDY to TiO_2) upon excitation of H-GDY. In turn, these two available pathways are expected to make the hydrogen evolution reaction more efficient.

To further elucidate and confirm the interfacial charge transfer between TiO_2 and H-GDY (GDY), a TRMC analysis was performed under laser-pulsed excitation at 360 nm, which enables exciton generation in both materials. Compared to the well-known photoluminescence time-resolved measurements, TRMC enables evaluating the dynamics of charge carriers in TiO_2-based composites.[47,48] Upon laser excitation of

the samples, the concentration of the photogenerated charge carriers increased during the pulse, and then a subsequent decay is observed owing to the decrease in the amount of excess charges, either by recombination, trapping, or surface reaction processes. It is worth noting that no TRMC signal was observed for pristine H-GDY (GDY), probably owing to the low sensitivity of the change in the conductivity of the carbon-based material. As shown in Figure 5e, pure TiO_2 shows a higher maximum value of the signal compared to GDY/TiO_2 and H-GDY/TiO_2, which is probably attributed to the shield effect.[49,50] However, these effects, usually harmful for the photoactivity, can be compensated by the influence on the charge carriers' lifetime (decay), a liming factor in the photocatalytic reaction.

In contrast to pure TiO_2, GDY/TiO_2 and H-GDY/TiO_2 exhibited much slower global decay, leading to a higher number of charge carriers exploitable for photocatalytic reactions. Notably, a lifetime of charge carriers of ≈0.33 µs was observed in H-GDY/TiO_2, much longer than that for GDY/TiO_2 (≈0.24 µs), thus indicating that the heterojunction between H-GDY and TiO_2 is more efficient for the charge separation than that between GDY and TiO_2, in full consistency with the theoretical analysis and experimentally observed photocatalytic activity. Even if the charge carrier density produced at the TiO_2 surface is high, their lifetime is reduced owing to the fast recombination occurring right after the excitation. As the photocatalytic reaction takes a place over a much longer time scale, hybridizing TiO_2 with GDY and HGDY contributes in increasing the charge carrier lifetime via the charge separation process. The longer lifetime of charge carriers for H-GDY/TiO_2 under 420 nm laser-pulsed excitation, further proved the efficient interfacial charge separation under visible light (Figure S11, Supporting Information). All in all, the charge carrier separation in the H-GDY/TiO_2 and GDY/TiO_2 photocatalysts can be rationalized in the following way: GDY acts solely as a hole transport layer, while the H-substitution enables to markedly increase the bandgap and provide a proper positioning of the CB and VB bands to construct an efficient type II heterojunction with TiO_2; this fully promotes a full charge carrier separation (Figure 5f), which subsequently improves the photocatalytic activity toward H_2 generation.

3. Conclusions

In conclusion, the electronic bandgap of GDY was adjusted by H-substitution and the obtained H-GDY was hybridized with TiO_2 to form a type II heterojunction. The prepared H-GDY/TiO_2 displayed excellent photocatalytic activity with H_2 production rate of ≈6200 µmol h^{-1} g^{-1} under UV–visible illumination and ≈670 µmol h^{-1} g^{-1} under visible illumination, which were 1.35 and 4 times higher than that of GDY/TiO_2 composite, respectively. DFT calculations revealed that the superior activity of H-GDY is attributed to the suitable band alignment between H-GDY and TiO_2, which promote photogenerated electron and hole separation via different pathways compared to the GDY/TiO_2 heterojunction. TRMC evidenced the longest lifetime of charge carriers in H-GDY/TiO_2, further evidencing the successful fabrication of type II heterojunction. The concept of tuning the electronic bandgap of GDY to construct efficient heterojunctions enhancing interfacial carrier separation is certainly not confined to H-substitution and TiO_2 but should be extended to other element doping and semiconductors for photocatalytic applications. Related works are in progress in the laboratory.

Supporting Information

Supporting Information is available from the Wiley Online Library or from the author.

Acknowledgements

J.L. acknowledges the public grant overseen by the French National Research Agency (ANR) as part of the "Investissements d'Avenir" program (Labex NanoSaclay, reference: ANR-10-LABX-0035) for his post-doc position. The work in Mons was supported by the Belgian National Fund for Scientific Research (FRS-FNRS). Computational resources were provided by the Consortium des Équipements de Calcul Intensif (CÉCI) funded by F.R.S.-FNRS under Grant No. 2.5020.11. J.C. is an FNRS research director. ICN2 acknowledges funding from Generalitat de Catalunya 2017 SGR 327 and the Spanish MINECO project ENE2017-85087-C3. ICN2 was supported by the Severo Ochoa program from Spanish MINECO (Grant No. SEV-2017-0706) and was funded by the CERCA Programme/Generalitat de Catalunya. Part of the present work was performed in the framework of Universitat Autònoma de Barcelona Materials Science Ph.D. program. X.H. thanks China Scholarship Council for scholarship support (201804910551). The authors are grateful to François Devred for his help in performing the XPS experiments.

Conflict of Interest

The authors declare no conflict of interest.

Data Availability Statement

The data that support the findings of this study are available from the corresponding author upon reasonable request.

Keywords

charge carrier, density functional theory, electronic bandgaps, graphdiyne, photocatalysis

Received: January 29, 2021
Revised: March 1, 2021
Published online:

[1] X. Yang, D. Wang, *ACS Appl. Energy Mater.* **2018**, *1*, 6657.
[2] C. Xu, P. R. Anusuyadevi, C. Aymonier, R. Luque, S. Marre, *Chem. Soc. Rev.* **2019**, *48*, 3868.
[3] C. Dai, B. Liu, *Energy Environ. Sci.* **2020**, *13*, 24.
[4] H. Wang, L. Zhang, Z. Chen, J. Hu, S. Li, Z. Wang, J. Liu, X. Wang, *Chem. Soc. Rev.* **2014**, *43*, 5234.
[5] J. Li, P. Jiménez-Calvo, E. Paineau, M. N. Ghazzal, *Catalysts* **2020**, *10*, 89.
[6] W. Zhu Li, C. Li, T. Wang, J. Gong, *Chem. Soc. Rev.* **2019**, *48*, 1874.

[7] J.-X. Li, Z.-J. Li, C. Ye, X.-B. Li, F. Zhan, X.-B. Fan, J. Li, B. Chen, Y. Tao, C.-H. Tung, L.-Z. Wu, *Catal. Sci. Technol.* **2016**, *6*, 672.
[8] T. Umeyama, H. Imahori, *Energy Environ. Sci.* **2008**, *1*, 120.
[9] S. Ye, C. Ding, R. Chen, F. Fan, P. Fu, H. Yin, X. Wang, Z. Wang, P. Du, C. Li, *J. Am. Chem. Soc.* **2018**, *140*, 3250.
[10] S. Bellani, L. Najafi, B. Martín-García, A. Ansaldo, A. E. Del Rio Castillo, M. Prato, I. Moreels, F. Bonaccorso, *J. Phys. Chem. C* **2017**, *121*, 21887.
[11] U. Sim, J. Moon, J. An, J. H. Kang, S. E. Jerng, J. Moon, S.-P. Cho, B. H. Hong, K. T. Nam, *Energy Environ. Sci.* **2015**, *8*, 1329.
[12] X. Gao, H. Liu, D. Wang, J. Zhang, *Chem. Soc. Rev.* **2019**, *48*, 908.
[13] C. Huang, Y. Li, N. Wang, Y. Xue, Z. Zuo, H. Liu, Y. Li, *Chem. Rev.* **2018**, *118*, 7744.
[14] J. Li, X. Gao, L. Zhu, M. N. Ghazzal, J. Zhang, C.-H. Tung, L.-Z. Wu, *Energy Environ. Sci.* **2020**, *13*, 1326.
[15] H. Yu, Y. Xue, Y. Li, *Adv. Mater.* **2019**, *31*, 1803101.
[16] J. Li, X. Gao, Z. Li, J.-H. Wang, L. Zhu, C. Yin, Y. Wang, X.-B. Li, Z. Liu, J. Zhang, C.-H. Tung, L.-Z. Wu, *Adv. Funct. Mater.* **2019**, *29*, 1808079.
[17] J. Li, X. Gao, X. Jiang, X.-B. Li, Z. Liu, J. Zhang, C.-H. Tung, L.-Z. Wu, *ACS Catal.* **2017**, *7*, 5209.
[18] R. Sakamoto, N. Fukui, H. Maeda, R. Matsuoka, R. Toyoda, H. Nishihara, *Adv. Mater.* **2019**, *31*, 1804211.
[19] N. Wang, J. He, K. Wang, Y. Zhao, T. Jiu, C. Huang, Y. Li, *Adv. Mater.* **2019**, *31*, 1803202.
[20] X. P. Yin, H. J. Wang, S. F. Tang, X. L. Lu, M. Shu, R. Si, T. B. Lu, *Angew. Chem., Int. Ed.* **2018**, *57*, 9382.
[21] N. Yang, Y. Liu, H. Wen, Z. Tang, H. Zhao, Y. Li, D. Wang, *ACS Nano* **2013**, *7*, 1504.
[22] S. Thangavel, K. Krishnamoorthy, V. Krishnaswamy, N. Raju, S. J. Kim, G. Venugopal, *J. Phys. Chem. C* **2015**, *119*, 22057.
[23] J.-X. Lv, Z.-M. Zhang, J. Wang, X.-L. Lu, W. Zhang, T.-B. Lu, *ACS Appl. Mater. Interfaces* **2019**, *11*, 2655.
[24] Q. Xu, B. Zhu, B. Cheng, J. Yu, M. Zhou, W. Ho, *Appl. Catal., B* **2019**, *255*, 117770.
[25] R. Wang, M. Shi, F. Xu, Y. Qiu, P. Zhang, K. Shen, Q. Zhao, J. Yu, Y. Zhang, *Nat. Commun.* **2020**, *11*, 4465.
[26] F. Xu, K. Meng, B. Zhu, H. Liu, J. Xu, J. Yu, *Adv. Funct. Mater.* **2019**, *29*, 1904256.
[27] G. Luo, X. Qian, H. Liu, R. Qin, J. Zhou, L. Li, Z. Gao, E. Wang, W.-N. Mei, J. Lu, Y. Li, S. Nagase, *Phys. Rev. B* **2011**, *84*, 075439.
[28] M. Long, L. Tang, D. Wang, Y. Li, Z. Shuai, *ACS Nano* **2011**, *5*, 2593.
[29] T. Su, Q. Shao, Z. Qin, Z. Guo, Z. Wu, *ACS Catal.* **2018**, *8*, 2253.
[30] J. Wang, S. Lin, N. Tian, T. Ma, Y. Zhang, H. Huang, *Adv. Funct. Mater.* **2021**, *31*, 2008008.
[31] H. Wang, B. Zhang, F. Zhao, B. Zeng, *ACS Appl. Mater. Interfaces* **2018**, *10*, 35281.
[32] U. Sim, T.-Y. Yang, J. Moon, J. An, J. Hwang, J.-H. Seo, J. Lee, K. Y. Kim, J. Lee, S. Han, B. H. Hong, K. T. Nam, *Energy Environ. Sci.* **2013**, *6*, 3658.
[33] S. Zhao, D.-W. Wang, R. Amal, L. Dai, *Adv. Mater.* **2019**, *31*, 1801526.
[34] H. Jin, C. Guo, X. Liu, J. Liu, A. Vasileff, Y. Jiao, Y. Zheng, S.-Z. Qiao, *Chem. Rev.* **2018**, *118*, 6337.
[35] G. Li, Y. Li, H. Liu, Y. Guo, Y. Li, D. Zhu, *Chem. Commun.* **2010**, *46*, 3256.
[36] J. Zhou, X. Gao, R. Liu, Z. Xie, J. Yang, S. Zhang, G. Zhang, H. Liu, Y. Li, J. Zhang, Z. Liu, *J. Am. Chem. Soc.* **2015**, *137*, 7596.
[37] H. Shang, Z. Zuo, H. Zheng, K. Li, Z. Tu, Y. Yi, H. Liu, Y. Li, Y. Li, *Nano Energy* **2018**, *44*, 144.
[38] Y. Zhao, J. Wan, H. Yao, L. Zhang, K. Lin, L. Wang, N. Yang, D. Liu, L. Song, J. Zhu, L. Gu, L. Liu, H. Zhao, Y. Li, D. Wang, *Nat. Chem.* **2018**, *10*, 924.
[39] Y. Kong, J. Li, S. Zeng, C. Yin, L. Tong, J. Zhang, *Chem* **2020**, *6*, 1933.
[40] C. Xing, Y. Xue, B. Huang, H. Yu, L. Hui, Y. Fang, Y. Liu, Y. Zhao, Z. Li, Y. Li, *Angew. Chem., Int. Ed.* **2019**, *58*, 13897.
[41] S. Zhuo, Y. Shi, L. Liu, R. Li, L. Shi, D. H. Anjum, Y. Han, P. Wang, *Nat. Commun.* **2018**, *9*, 3132.
[42] T. Zhang, Y. Hou, V. Dzhagan, Z. Liao, G. Chai, M. Loffler, D. Olianas, A. Milani, S. Xu, M. Tommasini, D. R. T. Zahn, Z. Zheng, E. Zschech, R. Jordan, X. Feng, *Nat. Commun.* **2018**, *9*, 1140.
[43] H. Pan, H. Zhang, H. Wang, J. Li, Y. Sun, W. Lu, X. Wang, *Appl. Surf. Sci.* **2020**, *513*, 145694.
[44] Q. Lv, W. Si, J. He, L. Sun, C. Zhang, N. Wang, Z. Yang, X. Li, X. Wang, W. Deng, Y. Long, C. Huang, Y. Li, *Nat. Commun.* **2018**, *9*, 3376.
[45] T. R. Gordon, M. Cargnello, T. Paik, F. Mangolini, R. T. Weber, P. Fornasiero, C. B. Murray, *J. Am. Chem. Soc.* **2012**, *134*, 6751.
[46] W. Jiao, L. Wang, G. Liu, G. Q. Lu, H.-M. Cheng, *ACS Catal.* **2012**, *2*, 1854.
[47] G. D. Gesesse, T. Le Neel, Z. Cui, G. Bachelier, H. Remita, C. Colbeau-Justin, M. N. Ghazzal, *Nanoscale* **2018**, *10*, 20140.
[48] C. Wang, J. Li, E. Paineau, A. Laachachi, C. Colbeau-Justin, H. Remita, M. N. Ghazzal, *J. Mater. Chem. A* **2020**, *8*, 10779.
[49] A. Nakayama, S. Hoshino, Y. Yamada, A. Ohmura, F. Ishikawa, *Appl. Phys. Lett.* **2015**, *107*, 231604.
[50] C. Zhou, Y. Yang, Y. Zhu, J. Ma, J. Long, R. Yuan, Z. Ding, Z. Li, C. Xu, *Catal. Sci. Technol.* **2018**, *8*, 4734.